

# A beam profile monitor for GeV photon with high spatial resolution and fast readout capability

R. Kino<sup>a,b,1</sup>, T. Akiyama<sup>a,b</sup>, H. Fujioka<sup>d</sup>, T. Fujiwara<sup>a</sup>, T. Ishige<sup>a,b</sup>,  
 K. Itabashi<sup>e</sup>, S. Kajikawa<sup>a,b</sup>, M. Kaneta<sup>a</sup>, M. Mizuno<sup>a</sup>, S. Nagao<sup>c</sup>,  
 S.N. Nakamura<sup>c</sup>, K. Nishi<sup>c</sup>, K. Nishida<sup>c</sup>, K. Okuyama<sup>a,b</sup>, F. Oura<sup>a,b</sup>,  
 K. Tachibana<sup>a,b</sup>, Y. Toyama<sup>f</sup>, D. Watanabe<sup>a</sup>

<sup>a</sup>Graduate School of Science, Tohoku University, Sendai, 980-8578, Japan

<sup>b</sup>Graduate Program on Physics for the Universe (GP-PU), Tohoku University, Sendai, 980-8578, Japan

<sup>c</sup>Graduate School of Science, The University of Tokyo, Tokyo, 113-0033, Japan

<sup>d</sup>School of Science, Tokyo Institute of Technology, Tokyo, 152-8550, Japan

<sup>e</sup>International Center for Quantum-field Measurement Systems for Studies of the Universe and Particles, Tsukuba, 305-0801, Japan

<sup>f</sup>Center for Muon Science and Technology, Chubu University, Nagoya, 487-8501, Japan

---

## Abstract

A beam profile monitor (BPM) has been developed to measure photon beams at the BM4 beamline of the Mikamine site, Research Center for Accelerator and Radioisotope Science (RARIS-Mikamine; previously known as ELPH) at Tohoku University. The BPM comprises plastic scintillation fibers and SiPMs, enabling high-precision, real-time measurements of photon beams in the 1 GeV region. Data acquisition utilized streaming TDC, a firmware commonly employed in the J-PARC Hadron-hall, enabling real-time detection of high-intensity photon beams with count rates reaching several tens of MHz. With sufficient statistical data, the BPM achieved a 1 s beam-profiling accuracy of 10  $\mu\text{m}$ . The proposed BPM serves as a valuable resource for future physics experiments at the BM4 photon beamline and will contribute significantly to ongoing accelerator research endeavors.

*Keywords:* beam profile, tagged photon, SiPM, scintillation fiber, streaming TDC

---

## 1. Introduction

In several physics experiments using particle accelerators, it is crucial to gain a comprehensive understanding of the properties of the beams generated by these accelerators. Such understanding facilitates the collection of higher-quality physics data and improves the tuning and performance of the accelerators.

At the Research Mikamine site, Research Center for Accelerator and Radioisotope Science (RARIS-Mikamine; previously known as ELPH) at Tohoku University, the electron synchrotron BST ring produces bremsstrahlung photon beams in the 1 GeV region[1]. The BST ring accelerates electrons initially injected with an energy of 90 MeV up to 1.3 GeV, where they are stored within the ring. The injection cycle lasts approximately 17 s, and during typical operation, a flat-top phase of approximately 10 s is established[2].

To generate a bremsstrahlung photon beam, a  $\phi 11 \mu\text{m}$  carbon fiber radiator is inserted into the path of orbiting electrons during the flat-top phase. This radiator synchronously moves along with the accelerator's operation and remains stationary at a location distant from the electron orbit. As the electrons are injected and accelerated within the BST ring, the radiator gradually shifts toward the center of the electron intensity distribution on the flat-top phase. Following the conclusion of the flat-top phase, the radiator is immediately removed from the electron orbit, with its precise operation controlled by a stepping motor[3].

The BST ring accommodates two photon beamlines, namely, BM4 and BM5. BM4 beamline is equipped with an electromagnetic spectrometer, NKS2 [4], while BM5 beamline has an electromagnetic calorimeter known as FOREST[5]. Both beamlines are equipped with photon energy tagging devices referred to as Taggers[3, 6]. These Taggers can identify the energy of the photon beam by measuring the timing and position of the scattering electrons generated by bremsstrahlung, all without disrupting the photons.

The 1 GeV region photon beam, tagged using this method, proves useful for investigating hadrons, including strangeness nuclear physics, and several experiments have been conducted on this beamline. Accurate beam profiling is

necessary for several reasons, such as measuring reaction points and designing the positions of detectors and targets. Additionally, the accuracy of the beam profile significantly affects the final physical results.

Previous methods employed for profiling photon beams at the BM4 beamline have proven insufficient in meeting the accuracy requirements of these physical experiments. Two distinct tools have been used to ascertain the beam profile:

The first method involves the use of instant camera film (Fujifilm, Instax), operating on the principles of an emulsion plate. In this method, the beam is directed onto the film, and a photograph is developed using a camera subsequent to stopping the extraction beam and the operation of the BST ring. However, this method suffers from the following disadvantages: (1) it lacks the capability to quantitatively measure the beam profile, and (2) it necessitates a considerable amount of time to visualize the profile.

The second method uses the high-speed beam position monitor (HSBPM [7]), which is a detector employing scintillation fibers (Sci-Fi) (Saint-Gobain, BCF-10SC,  $\phi 3.0$  mm) and a multi-anode PMT (Hamamatsu Photonics K.K., H6568-10MOD). This HSBPM incorporates two types of plastic scintillators for the VETO counter of charged particle backgrounds and the trigger counter, an aluminum photon converter for generating electron-positron pairs from a portion of the photon beam, and Sci-Fi layers for precise particle position determination. While this detector offers the ability to quantitatively measure the photon-beam profile, its size and Sci-Fi segments limit its usage exclusively downstream (at a distance of approximately 10 m) of the beamline.

For these reasons, a novel photon-beam profile monitoring system has been developed. This new system permits real-time monitoring and quantitative evaluation and can be used at three distinct points within the beamline, including upstream, midstream, and downstream locations. In this paper, we present the development of this new Beam Profile Monitor (BPM) designed specifically for high-energy and intensity photon beams.

## 2. System for detecting photons which are neutral particles

The primary structure of the BPM comprises scintillation fibers (Sci-Fi) and SiPMs, employed for the detection of photon beams composed of neutral particles. The detection component of the BPM features a five-layer structure, as illustrated in the schematic in Figure 1. This section provides an explanation for each layer.

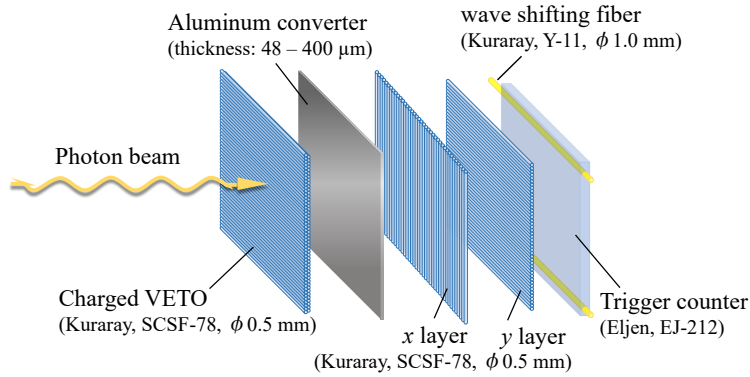


Figure 1: Schematic diagram of the particle detection portion which is composed of five layers in order from the upstream of the beam. The first layer is the veto counter (Section 2.1) used to detect the background of charged particles. The second layer is the aluminum photon converter (Section 2.2) responsible for generating electron-positron pair production from a part of the photon beam. The third and fourth layers are the Sci-Fi layers (Section 2.3) used to determine the particle position. The fifth layer is the trigger counter (Section 2.4) used for event identification. The effective area for detection is  $22.5 \times 22.5 \text{ mm}^2$ .

### 2.1. Charged VETO counter for removing charged backgrounds

The upstream counter within the beam serves as a VETO counter designed to detect charged particles, which represent background events within the laboratory. When generated at the radiator position, the photon beam interacts with substances such as air and aluminum flange, forming electron-positron pairs. Therefore, to accurately profile the photon beam, effectively mitigating the background of charged particles with this charged VETO counter becomes

essential. However, it is crucial to avoid excessive material thickness, as it can lead to unnecessary electron-positron pair production within the detector. Striking a balance between these requirements, we used 99 scintillation fibers (Kuraray, SCSF-78) with a diameter of 0.5 mm for the charged VETO counter, arranging them in double layers to eliminate gaps. This design enabled efficient detection of charged particle background while keeping material thickness in check. The effective thickness in the beam's direction for this counter is approximately 0.93 mm, and the photon conversion probability stands at approximately 0.17 %.

We bundled 33 scintillation fibers and connected them to three multipixel photon counters (MPPCs) (Hamamatsu K.K., S13360-3050PE) linked in parallel.

### *2.2. Aluminum photon converter*

The subsequent layer is the photon converter, consisting of a thin aluminum plate with a thickness ranging from 48 to 400  $\mu\text{m}$ . Its primary function is to generate electron-positron pairs from a small fraction of the photon beam, which ranges from 0.04 to 0.37 %. The ensuing Sci-Fi layers immediately detect the generated electron-positron pairs to determine the position of the incident particle. Minimizing the distance between the photon converter and Sci-Fi layers is crucial for mitigating the effect of multiple hits. To achieve this, the distance between the photon converter and Sci-Fi layers was reduced to 0.5 mm or less.

### *2.3. Fiber layers for determining particle position*

The next two layers consist of Sci-Fi fibers with a diameter of 0.5 mm (Kuraray, SCSF-78). These layers comprise 45 fibers arranged in both the direction of gravity ( $x$  channel) and the horizontal direction ( $y$  channel), and they serve the purpose of determining the positions of particles within the beam. The use of 0.5 mm diameter fibers helps in reducing the effective thickness of the detector along the beam axis, thereby suppressing excessive electron-positron pair production.

At the end of each fiber, three fibers are bundled together, and their tips make contact with the MPPCs (Hamamatsu K.K., S13360-1350PE). Each channel has a width of 1.5 mm, with a total of 15 channels in both the vertical and horizontal directions. This configuration ensures sufficient efficiency and accuracy for profiling a photon beam with a sigma value of approximately 1.5 mm.

#### 2.4. Trigger counter for event identification

The final layer within the detection section is the trigger counter, responsible for event identification. It employs a 2.0 mm thick plastic scintillator plate (Eljen, EJ-212) to ensure that no events are missed. Wavelength shifting fibers (Kuraray, Y-11,  $\phi$ 1.0 mm) are embedded at both ends of the scintillator plate, and the resulting scintillation light is detected by two MPPCs (Hamamatsu K.K., S13360-1350PE) connected in parallel.

All counters are connected to the MPPCs, detecting the scintillation light as a signal, which is then processed into a digital signal (as described in section 3.1) and collected using the Hadron Universal Logic (HUL) time-to-digital converter referred to as streaming TDC (also described in section 3.2). Once all the data has been recorded, events are identified offline by applying the conditions outlined in the following formula:

$$\begin{aligned} \text{Photon event} &= \overline{[\text{Charged VETO}]} \otimes [x \text{ layer}] \\ &\quad \otimes [y \text{ layer}] \otimes [\text{Trigger}] \end{aligned} \tag{1}$$

An event is defined as the time difference between the trigger counter and the  $x$ - and  $y$ -channels, with the charged VETO counter falling within the specified time window of 48 ns. This method ensures effective detection of neutral-photon beams.

The complete five-layer detector system was securely mounted on a specially designed acrylonitrile butadiene styrene (ABS) resin frame, as depicted in Figure 2. An original circuit board was developed to align the MPPCs, which read the

signals, with the fiber spacing. Both the board and fibers were firmly affixed to the frame to ensure stable and accurate measurements.

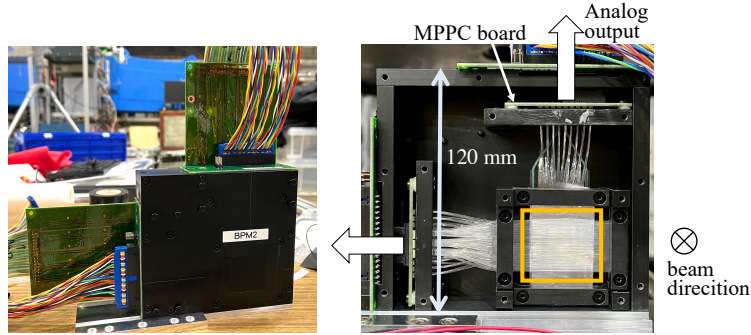


Figure 2: The exterior (left) and interior (right) of the developed BPM. The frame is made of black ABS resin, which is easy to process and has excellent impact resistance. The detection part is the part surrounded by the square in the right figure. Each MPPCs are fixed in contact with the end face of each fiber. The MPPC’s analog output signals are sent to the signal processing circuit (Section 3) outside the frame.

### 3. Readout and signal processing system

This section describes the readout and signal processing systems for the data obtained from the high-intensity photon beam. A circuit was developed (Section 3.1) to convert the analog output signals from the MPPCs into a format suitable for the data acquisition module (Section 3.2). Section 3.3 provides an overarching view of the data acquisition process.

#### 3.1. Signal amplifier and converter circuit

To accurately read the signal from the MPPCs, it is necessary to amplify the analog signal to an optimal level and convert it into a digital differential signal. For this purpose, a dedicated reading circuit was devised, as shown in Figure 3. The circuit encompasses an amplifier, employing an operational amplifier (Analog Devices, AD8000YRDZ) to amplify the MPPC signal approximately 20-fold, and a conversion circuit, which employs a high-speed comparator (Linear

Technology, LTC6754) to convert the signal into an LVDS signal. A similar circuit was replicated for all 32 channels per BPM.

The digital conversion method utilized the time over threshold (ToT) method, which converts wave height information into time information and measures it. In this method, the digital output contains time information at the leading edge and energy information corresponding to the pulse width. This allows for the simultaneous acquisition of time and energy information using a single signal line, reducing the circuit size of the data acquisition system and simplifying the configuration, ultimately reducing the overall cost. The HUL firmware (Section 3.2), used as the data acquisition module, accepts event durations within 4-150 ns. To maximize the use of this time range, we shaped the analog signal such that the median pulse width was approximately 80 ns.

The digital conversion comparator LTC6754 incorporates internal hysteresis, which can be adjusted within the range of 0-40 mV based on the value of the connected external resistor. In our developed conversion circuit, the hysteresis was configured at 40 mV. The output corresponding to one photoelectron (one pixel of the MPPC) was about 45 mV. For the  $x$  and  $y$  layers, the digital conversion threshold voltage ( $V_{th}$ ) was set to 280 mV, corresponding to 5-6 p.e. (photoelectrons), approximately half the average photon number.  $V_{th}$  for the Charged VETO and Trigger counters were set to 70 and 90 mV, respectively, to prevent oscillations due to noise.

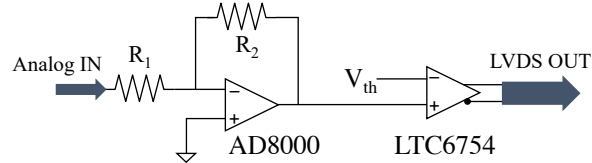


Figure 3: Schematic diagram of a signal amplifier circuit for one channel. The small analog signal output from the MPPC is amplified by a non-inverting amplifier circuit that includes the AD8000 operational amplifier. It is then converted into a digital differential signal via the high-speed comparator, LTC6754.



### 3.2. Streaming TDC

The primary module used for data acquisition was the HUL [8], an FPGA module commonly used in recent nuclear experiments. For data acquisition, we implemented a newly developed time-to-digital converter referred to as a streaming TDC [9], which facilitated triggerless continuous timing measurements. This firmware achieved a high dynamic range of approximately  $10^{10}$  timing measurements using the heartbeat method, which periodically generated delimiter data. Each TDC channel had a width of 0.96 ns, and it could collect continuous data for up to 32 s, rendering it suitable for profiling high-intensity photon beams with a counting rate of several MHz.

The integration of the streaming TDC enabled us to measure the tagged photon beams at counting rates of several MHz. Since all counter timestamps can be recorded without selection by online triggers, the desired data can be chosen after the data acquisition is complete, as shown in Eq. 1.

### 3.3. Data acquisition system

Figure 4 presents a block diagram that outlines the entire process of data acquisition. It is important to note that the gate signal needed to be supplied separately to the HUL, utilized for data acquisition, from the data signal. The streaming TDC continued to acquire data only when the gate signal was active. To synchronize with the photon beam, we employed a gate signal that became active when the internal radiator was in motion. Communication between the HULs and computers for data acquisition occurred through Ethernet using SiTCs technology [10]. In the actual test experiment, one computer simultaneously controlled four HULs, and data acquisition was performed accordingly.

## 4. Measured Photon Profiles

### 4.1. Setup for the test experiment

The experimental setup used in this study is illustrated in Figure 5. The coordinate system within the BM4 photon beamline was established with the y-

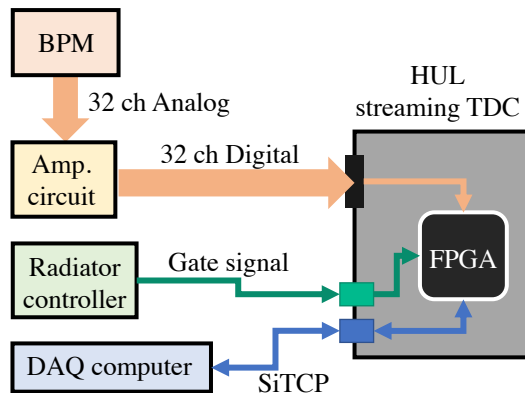


Figure 4: Schematic diagram of the data acquisition system. First, the signal obtained from the BPM is amplified by an amplifier circuit and converted into a digital differential signal, which is then input to the HUL as an LVDS signal. On the other hand, the gate signal synchronized with the movement of the radiator is input independently to the HUL from the radiator controller, which enables data acquisition synchronized with the photon beam. The DAQ computer and HUL communicate with each other via SiTCP.

axis pointing opposite to the gravitational direction, the  $z$ -axis aligned with the direction of the photon beam, and the  $x$ -axis perpendicular to both the  $y$  and  $z$ -axes. The  $x$ -axis pointed toward the inside of the BST ring, following the right-handed system convention. Two new BPMs, BPM1 and BPM2, were developed and installed on the beamline to monitor the photon beams. BPM1 possesses the capability to move in the  $x$  and  $z$ -directions using two movable stages and can be remotely controlled to position in front or behind the collimator. BPM2 remained fixed at the entrance of the NKS2 spectrometer.

Additionally, the existing HSBPM was installed as BPM3 downstream of the beamline. The entire DAQ system for BPM3 was replaced by a new system, incorporating a streaming TDC, akin to BPM1 and 2. The analog output signal from the multi-anode PMT was initially converted to an emitter coupled logic (ECL) signal utilizing an NIM standard discriminator ( $\text{GeV}\gamma-1380$ ). The digital conversion threshold voltage,  $V_{\text{th}}$ , was set to 40 mV, which corresponds to approximately 1/5th of the signal gain associated with the minimum en-

ergy loss (minimum ionization particle (MIP)) of a general plastic scintillator. Subsequently, the HUL collected data in the same manner as BPM1 and 2.

The entire data acquisition system comprised three HULs, each equipped with a StrTDC, independently reading 32 channels for each BPM. A gate signal synchronized with the movement of the radiator was simultaneously input to all HULs. A DAQ computer controlled all the HULs via SiTCP. The same DAQ computer also handled radiator control and BPM1 stage control. The typical data size for each HUL was as follows: BPM1: approximately 75 MB/spill, BPM2: approximately 55 MB/spill, BPM3: approximately 400 MB/spill. The typical data acquisition rates for each detector were BPM1: approximately 85 kHz, BPM2: approximately 54 kHz, BPM3: approximately 330 kHz (orbiting electron-beam current approximately 1 mA). StrTDC is capable of collecting time stamps at high rates, meaning that only 1 s of data acquisition is sufficient to obtain ample statistical data. Therefore, the beam-profiling system developed using these three BPMs can operate in real-time immediately after collecting data for one spill.

The distances of these BPM  $x$ -layers from the radiator were accurately measured using a laser rangefinder and were found to be 2.99, 5.66, and 10.13 m, respectively.

#### *4.2. Quantitative evaluation of beam profile*

Photon event selection was performed using Eq. 1 for the timestamps of all events recorded by the streaming TDC. The time window was set to  $\pm 48$  ns, effectively covering the difference in the timestamp between the trigger counter and each layer.

Figure 6 displays a typical beam profile, representing a 1-s profiling. The number of hits was presented as a histogram in both the horizontal and vertical directions, and a fitting process was performed using a function that incorporated two Gaussians (depicted using black lines in Figure 6). The blue line corresponds to the real beam structure, while the red line represents the beam's halo structure. It is conceivable that the origin of this halo structure lies in the

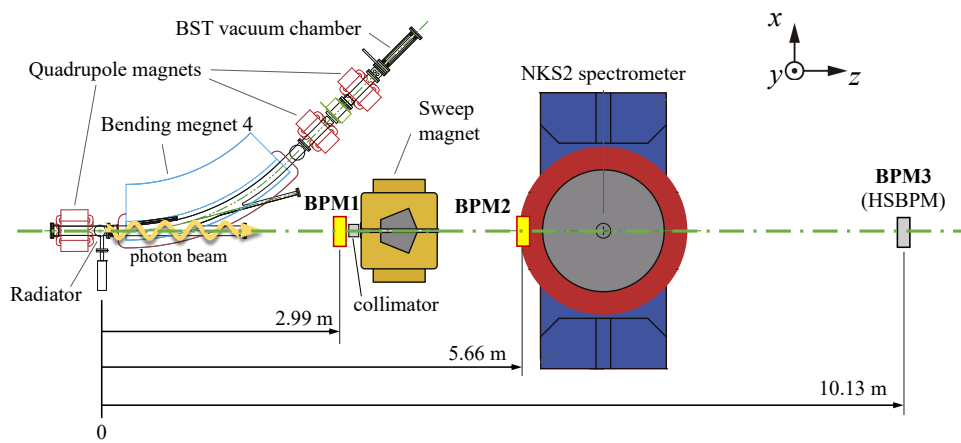


Figure 5: Schematic view of the BM4 beamline. The photon beam is generated at the radiator, located at the entrance of the dipole magnet, known as Bending Magnet 4. To minimize electron-positron background events, a Sweep magnet is also installed in the beamline. We have installed our newly developed Beam Profile Monitors (BPM1 and BPM2) in the up- and the mid-stream of the beamline. The BPM3(HSBPM) is placed at the most downstream point of the beamline.

charged particles generated at the aluminum flange, influenced by the efficiency of the charged VETO counter. The mean value ( $\mu$ , represented by the black dotted line) derived from the fitting was considered as the beam center position, while the sigma ( $\sigma$ ) was assessed as the beam size. The typical position accuracy was less than  $10 \mu\text{m}$  for the 1-s profile.

The gain of the MPPC output signal for each channel remained constant with an accuracy of 10%, which affected the detection efficiency by approximately 1%. However, the fluctuation resulting from this effect on the final profiling results was only a few micrometers, deemed negligible and carrying no significant impact on the reported values in this paper. Additionally, the error estimates for the values reported herein encompass solely the statistical errors obtained from chi-square fitting.

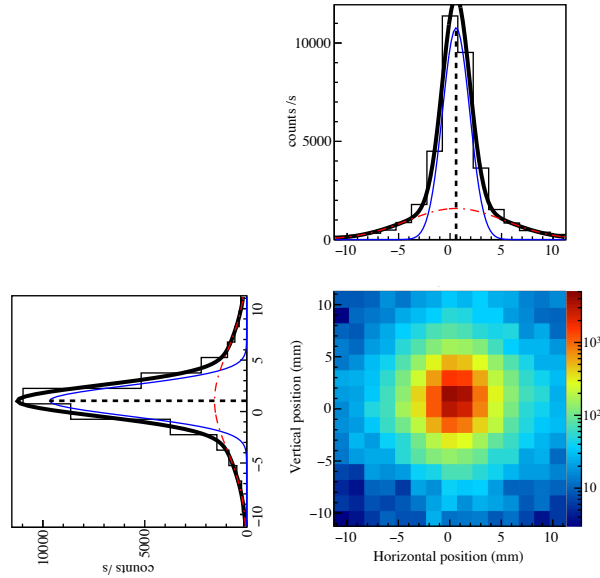


Figure 6: The two-dimensional distribution of hits in the  $x - y$  plane over a period of 1-s. The hits in the  $x$ -layer, corresponding to the horizontal direction, and the  $y$ -layer, corresponding to the vertical direction, are integrated and plotted. The blue line represents the real beam structure, while the red line represents the beam halo structure. The fitted function is a double Gaussian, represented by the black line, a sum of the blue and red lines.

### 4.3. Beam intensity dependence

The investigation of the photon-beam profile involved varying the electron-beam current within the BST ring. Since the beam current could not be directly measured, the beam intensity was evaluated using the measurement results obtained from the beam DCCT. Figure 7 shows the relationship between the beam position and intensity, revealing that there was no significant alteration in the beam position as the beam intensity increased. Figure 8 portrays dependency of the beam size on the beam intensity, where the beam size exhibited a minor increase as the beam intensity rose. This increase encompassed the effect of accidental background generated by the beam intensity. In scenarios with high beam intensity (count rate = 150 kHz), the beam size is estimated to be approximately 2% larger due to the influence of this accidental background.

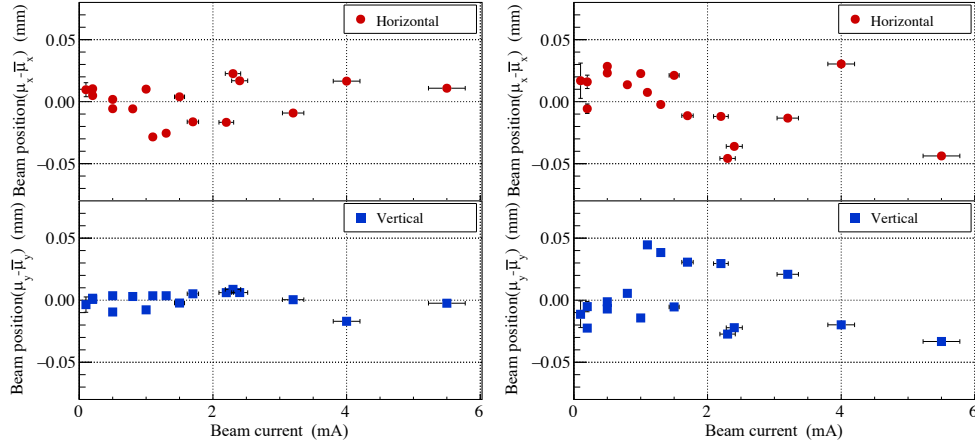


Figure 7: The dependence of the beam position on the beam intensity at two different points along the beamline. The figure on the left represents the position measurements from BPM1, which is located 2.99 m from the radiator, and the figure on the right represents measurements from BPM2, located 5.66 m from the radiator. The  $y$ -axis was set so that the average value ( $\bar{\mu}$ ) would be 0 for each. The red points in the figures represent the horizontal position of the beam, and the blue points represent the vertical position.

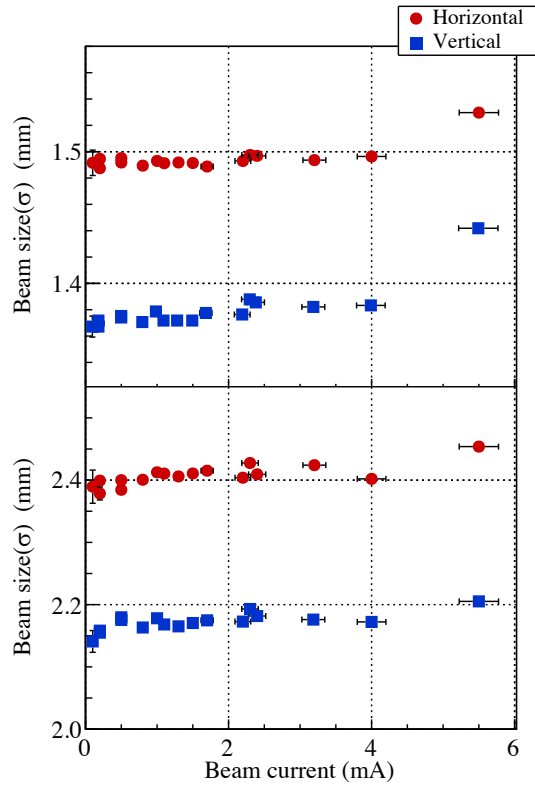


Figure 8: This figure shows the beam intensity dependence of the beam size, with BPM1 (at a distance of 2.99 m from the radiator) on the upper and BPM2 (at a distance of 5.66 m from the radiator) on the bottom. The red points represent the horizontal beam size, while the blue points represent the vertical beam size.

#### 4.4. Time dependence during a spill

Figure 9 shows the time variation of the beam profile during a spill. The plot demonstrates that the direction of the beam undergoes changes within a spill, with the horizontal variation consistent with the characteristics determined by the unique Twiss parameter of the BST ring and the  $x - x'$  phase space of the electron beam. The  $x - x'$  phase space defines the particle distribution and is typically determined by the Twiss parameters of the accelerator. At the radiator position in the BM4 beamline, the particle intensity within the  $x - x'$  phase space exhibits an opposite correlation, leading to the horizontal beam position moving in the opposite direction to the radiator's motion.

Furthermore, the plot suggests changes in the vertical direction, indicating that the  $x - y$  plane of the electron-beam position distribution at the radiator point is elliptically tilted. This phenomenon may be attributed to the alignment of the quadrupole magnets within the BST ring.

Figure 10 illustrates the time-dependent behavior of the beam size, indicating a significant increase during a spill. This phenomenon is attributed to the degradation of the electron-beam emittance caused by the insertion of a radiator. When the radiator moves within the electron beam, it induces electron scattering, which in turn degrades the emittance and enlarges the size of the photon beam [11]. The lower graph in Figure 10 shows the time-dependent behavior of the beam size measured using BPM3. This effect of electron scattering was not observed at greater distances from the radiator due to the larger original beam size.

#### 4.5. Radiator position dependence

During the operation of the BST ring, the radiator continually moves within a spill. To assess the dependence of the beam on the radiator position, the radiator was inserted at a specified point,  $x_{\text{rad}}$ , and then fixed in place after the electron beam was accelerated. The initial position of the radiator was recorded on both the outer and inner circumferences of the ring for both patterns, and the



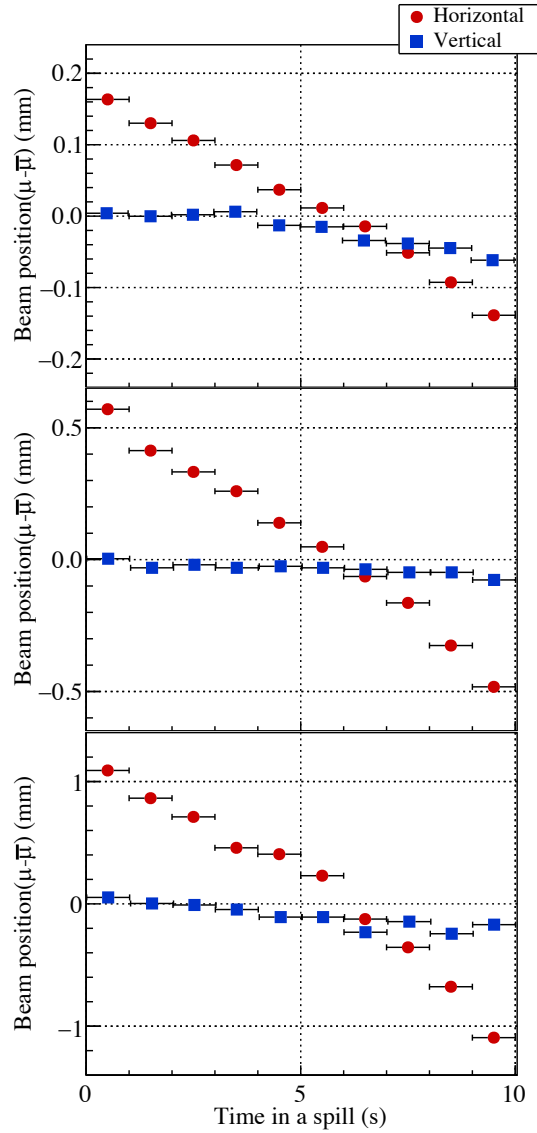


Figure 9: Time dependence of the beam position. The upper figure is measured by BPM1 (the distance from the radiator is 2.99 m), the middle is by BPM2 (the distance from the radiator is 5.66 m), and the bottom one is by BPM3 (the distance from the radiator is 10.13 m), respectively. The red points represent horizontal, and the blue ones represent vertical positions.

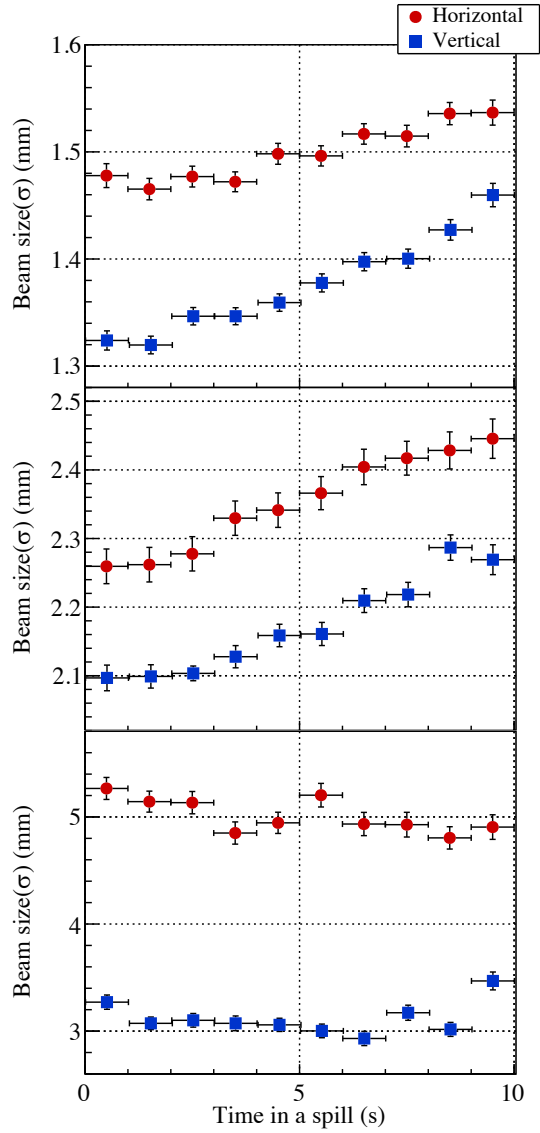


Figure 10: The time dependence of the beam size. The upper figure corresponds to BPM1 (the distance from the radiator is 2.99 m), the middle figure is BPM2 (the distance from the radiator is 5.66 m), and the bottom is measured by BPM3 (the distance from the radiator is 10.13 m), respectively. The red points represent the horizontal beam size, and the blue ones represent the vertical beam size.

results for both patterns are presented in the figures below. In these figures, the 0 point on the horizontal axis corresponds to the center of the electron beam.

Figure 11 shows the relationship between the beam center position and radiator position. The figure distinctly shows the correlation between the radiator's position and direction of the photon beam. Regarding the horizontal direction, the characteristics explained in the previous section related to the accelerator-specific Twiss parameter and  $x - x'$  phase space are clearly evident. A correlation in the vertical direction is also observed, confirming that the photon beam exhibits an upward behavior near the center of the electron beam.

Figures 12 and 13 show the dependence of the photon-beam size on the radiator position. The photon-beam size notably increases as the radiator approaches the center of the electron beam. The rate of increase in the vertical direction is more substantial because the emittance in the vertical direction is much smaller than that in the horizontal direction. Consequently, the effect of inserting the radiator is more pronounced in the vertical direction due to the smaller initial size of the beam in that direction [12]. The error bars in the positive radiator position area are larger because the radiator is inserted from the outer side of the BST ring, leading to most of the electron beam being intercepted before reaching the specified point  $x_{\text{rad}}$ , resulting in statistical errors.

During standard operation, the radiator moves within the range of -2.8 to -2.1 mm from the outer circumference to the inner circumference of the ring, aligning with the findings obtained from the time-dependent analysis (Section 4.4).

## 5. Summary

A novel BPM was developed to facilitate quantitative and real-time profiling of the photon beam at the RARIS-Mikamine BM4 photon beamline. This BPM employs plastic scintillation fibers and SiPMs as detectors, complemented by a VETO counter designed to remove charged particles and a photon converter enabling profiling of neutral-photon beams. The triggerless DAQ system,

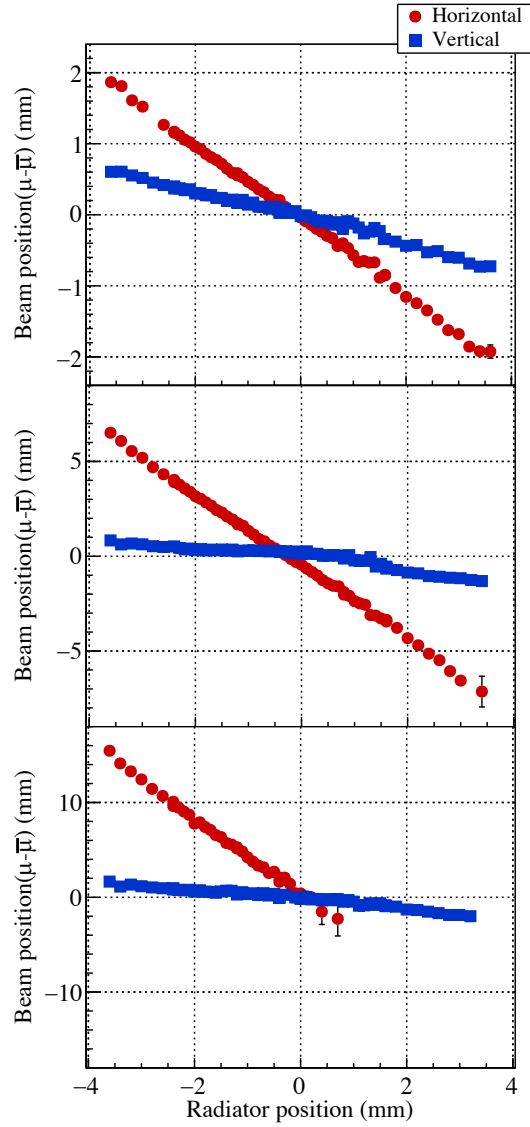


Figure 11: The radiator position dependence of the beam position. The upper figure is measured by BPM1(the direction from the radiator is 2.99 m), the middle is by BPM2(the direction from the radiator is 5.66 m), and the bottom is by BPM3(the direction from the radiator is 10.13 m), respectively. The red points represent the horizontal beam position, and the blue ones represent the vertical beam position. The 0 point on the vertical axis of BPM3 corresponds to the point when the horizontal axis is 0. The range of  $x_{\text{rad}} > 0.5$  mm is out of the detector's effective area.

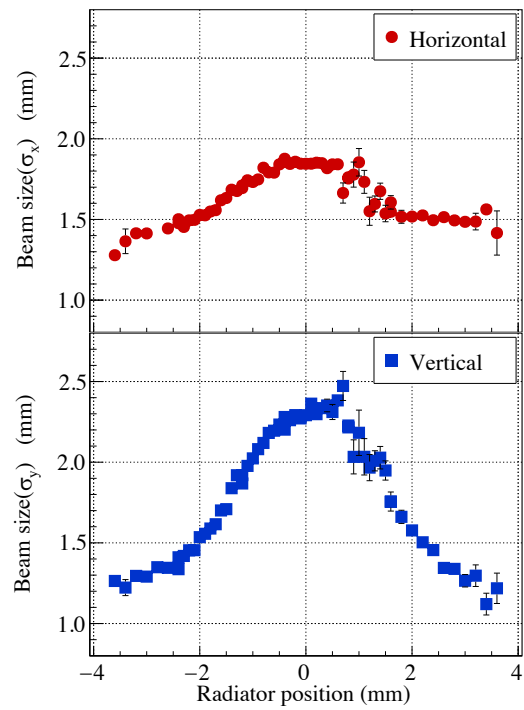


Figure 12: The dependence of the photon beam size on the position of the radiator at BPM1 (the direction from the radiator is 2.99 m). The red points represent the horizontal beam size, and the blue points represent the vertical beam size.

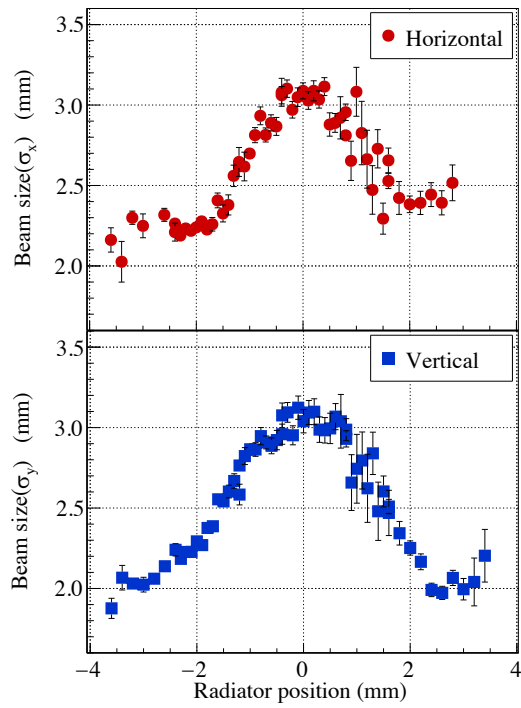


Figure 13: The dependence of the photon beam size on the position of the radiator at BPM2 (the direction from the radiator is 5.66 m). The red points represent the horizontal beam size, and the blue points represent the vertical beam size.

streaming TDC, enables the detection of high-intensity photon beams, exceeding several tens of MHz, with position measurements accurate to better than  $10\ \mu\text{m}$  for a 1-s beam profile.

Photon-beam measurements were performed under various conditions, revealing that the beam position remains unaffected by changes in beam intensity. However, it was observed that both the beam position and size exhibit a clear correlation with the radiator's position, resulting in time-dependent behavior during a spill.

This newly developed BPM serves as a valuable resource for future physics experiments at the BM4 photon beamline and will contribute significantly to ongoing accelerator research endeavors.

### **Acknowledgments**

The authors appreciate the staff of the RARIS-Mikamine accelerator for providing the primary electron beam and stable operation of the BST ring. In particular, we thank Prof. Fujio Hinode, Prof. Takatsugu Ishikawa, and Dr. Toshiya Muto for their discussions on the accelerator parameters and the behavior of electrons in the BST ring related to this measurement.

This work was supported by the RARIS-Mikamine (Proposal No. 2981 and No. 2982).

Financial support for this project was provided in part by JSPS KAKENHI Grant Number 18H05459 and 24H00219, and Grant-in-Aid for JSPS Fellows Number 23KJ0180. Five of the authors (RK, SK, KO, FO, and KT) acknowledge support from the JSPS Research Fellowship for Young Scientists.

## References

- [1] F. Hinode, T. Muto, M. Kawai, S. Kashiwagi, Y. Shibasaki, K. Nanbu, I. Nagasawa, K. Takahashi, H. Hama, Upgrade of the 1.2 gev stb ring for the sr utilization in tohoku university, *Journal of Physics: Conference Series* 425 (7) (2013) 072011.
- [2] T. U. Research center for Electron-Photon Science, ([url: https://www.lns.tohoku.ac.jp](https://www.lns.tohoku.ac.jp)).
- [3] H. Yamazaki, T. Kinoshita, K. Hirota, T. Katsuyama, T. Itoh, A. Kato, T. Nakabayashi, O. Konno, T. Takahashi, K. Maeda, J. Kasagi, [The 1.2 gev photon tagging system at lns-tohoku](#), *Nuclear Instruments and Methods in Physics Research Section A: Accelerators, Spectrometers, Detectors and Associated Equipment* 536 (1) (2005) 70–78. doi:<https://doi.org/10.1016/j.nima.2004.07.144>.  
URL <https://www.sciencedirect.com/science/article/pii/S0168900204016808>
- [4] M. Kaneta, B. Beckford, T. Fujii, Y. Fujii, K. Futatsukawa, Y. Han, O. Hashimoto, K. Hirose, T. Ishikawa, H. Kanda, C. Kimura, K. Maeda, S. Nakamura, K. Suzuki, K. Tsukada, F. Yamamoto, H. Yamazaki, [Neutral kaon spectrometer 2](#), *Nuclear Instruments and Methods in Physics Research Section A: Accelerators, Spectrometers, Detectors and Associated Equipment* 886 (2018) 88–103. doi:<https://doi.org/10.1016/j.nima.2017.12.076>.  
URL <https://www.sciencedirect.com/science/article/pii/S0168900217314948>
- [5] T. Ishikawa, H. Fujimura, H. Fukasawa, R. Hashimoto, T. Ishida, S. Kaida, J. Kasagi, A. Kawano, S. Kuwasaki, K. Maeda, F. Miyahara, K. Mochizuki, T. Nakabayashi, A. Nakamura, K. Nawa, S. Ogushi, Y. Okada, K. Okamura, Y. Onodera, Y. Saito, Y. Sakamoto, M. Sato, H. Shimizu, H. Sugai, K. Suzuki, S. Takahashi, Y. Tsuchikawa, H. Yamazaki, H. Yonemura, [The](#)



forest detector for meson photoproduction experiments at elph, Nuclear Instruments and Methods in Physics Research Section A: Accelerators, Spectrometers, Detectors and Associated Equipment 832 (2016) 108–143. doi:<https://doi.org/10.1016/j.nima.2016.06.054>.

URL <https://www.sciencedirect.com/science/article/pii/S0168900216305964>

- [6] T. Nishizawa, Y. Fujii, H. Kanda, M. Kaneta, Y. Kasai, J. Kusaka, K. Maeda, S. Nagao, S. N. Nakamura, K. Tsukada, F. Yamamoto, Development of a fast timing counter with a monolithic mppc array, IEEE Transactions on Nuclear Science 61 (3) (2014) 1278–1283. doi:[10.1109/TNS.2014.2321657](https://doi.org/10.1109/TNS.2014.2321657).

- [7] T. Ishikawa, H. Fujimura, H. Hamano, R. Hashimoto, Y. Honda, T. Ishida, S. Kaida, H. Kanda, S. Kido, Y. Matsumura, M. Miyabe, K. Mizutani, I. Nagasawa, A. Nakamura, K. Nanbu, K. Nawa, S. Ogushi, Y. Shibasaki, H. Shimizu, H. Sugai, K. Suzuki, K. Takahashi, S. Takahashi, Y. Taniguchi, A. Tokiyasu, Y. Tsuchikawa, H. Yamazaki, A fast profile monitor with scintillating fiber hodoscopes for high-intensity photon beams, Nuclear Instruments and Methods in Physics Research Section A: Accelerators, Spectrometers, Detectors and Associated Equipment 811 (2016) 124–132. doi:<https://doi.org/10.1016/j.nima.2015.12.027>.

URL <https://www.sciencedirect.com/science/article/pii/S0168900215015983>

- [8] H. U. L. Module, (url: <http://openit.kek.jp/project/HUL>)[in japanese].

- [9] R. Honda, T. Aramaki, H. Asano, T. Akaishi, W. C. Chang, Y. Igarashi, T. Ishikawa, S. Kajikawa, Y. Ma, K. Nagai, H. Noumi, H. Sako, K. Shirotori, T. Takahashi, Continuous timing measurement using a data-streaming DAQ system, Progress of Theoretical and Experimental Physics 2021 (12), 123H01 (10 2021). arXiv:<https://academic.oup.com/ptep/article-pdf/2021/12/123H01/42899334/ptab128.pdf>, doi:

[10.1093/ptep/ptab128](https://doi.org/10.1093/ptep/ptab128).

URL <https://doi.org/10.1093/ptep/ptab128>

- [10] T. Uchida, Hardware-based tcp processor for gigabit ethernet, *IEEE transactions on nuclear science* 55 (3) (2008) 1631–1637.
- [11] T. Muto, H. Hama, T. Ishikawa, H. Kanda, S. Kashiwagi, F. Hinode, K. Nanbu, I. Nagasawa, K. Takahashi, C. Tokoku, E. Kobayashi, H. Saito, Y. Shibasaki, Impact of coulomb scattering in radiator wire on bremsstrahlung gamma ray in an electron storage ring, *Proceedings of the 12th Annual Meeting of Particle Accelerator Society of Japan* (8 2015).
- [12] T. Muto, Private communication (2022).